WENO RECONSTRUCTIONS OF UNCONDITIONALLY OPTIMAL HIGH ORDER

ANTONIO BAEZA*, RAIMUND BÜRGER†, PEP MULET‡, AND DAVID ZORÍO§

Abstract. A modified Weighted Essentially Non-Oscillatory (WENO) reconstruction technique preventing accuracy loss near critical points (regardless of their order) of the underlying data is presented. This approach only uses local data from the reconstruction stencil and does not rely on any sort of scaling parameters. The key novel ingredient is a weight design based on a new smoothness indicator, which defines the first WENO reconstruction procedure that never loses accuracy on smooth data, regardless of the presence of critical points of any order, and is therefore addressed as optimal WENO (OWENO) method. The corresponding weights are non-dimensional and scale-independent. The weight designs are supported by theoretical results concerning the accuracy of the smoothness indicators. The method is validated by numerical tests related to algebraic equations, scalar conservation laws, and systems of conservation laws.

Keywords: Finite-difference schemes, WENO reconstructions, optimal order, critical points

Mathematics subject classifications (2000): 65M06

1. Introduction.

1.1. Scope. Weighted Essentially Non-Oscillatory (WENO) reconstructions, initially proposed by Liu et al. [14] and later improved by Jiang and Shu [12], have become a common ingredient of high-resolution schemes for the numerical solution of hyperbolic conservation laws. The standard initial-value problem is of the type

$$\boldsymbol{u}_t + \sum_{i=1}^{\mathcal{D}} \boldsymbol{f}_i(\boldsymbol{u})_{x_i} = \boldsymbol{0}, \quad \boldsymbol{x} = (x_1, \dots, x_{\mathcal{D}}) \in \mathbb{R}^{\mathcal{D}}, \quad t > 0, \tag{1.1}$$

where $\boldsymbol{u} = \boldsymbol{u}(\boldsymbol{x}, t) = (u_1, \dots, u_N)^{\mathrm{T}}$ is the vector of sought unknowns and $\boldsymbol{f}_i(\boldsymbol{u}) = (f_{i,1}(\boldsymbol{u}), \dots, f_{i,N}(\boldsymbol{u}))^{\mathrm{T}}$ are given flux vectors, supplied with an initial condition

$$\boldsymbol{u}(\boldsymbol{x}, 0) = \boldsymbol{u}_0(\boldsymbol{x}), \quad \boldsymbol{x} \in \mathbb{R}^{\mathcal{D}}. \tag{1.2}$$

Such schemes (in short, "WENO schemes") present a high order of accuracy in smooth zones and, through a sophisticated construction of non-linear weights [12], avoid the oscillatory behaviour typical of the reconstructions from discontinuous data. However, such weights are sensitive not only to discontinuities, but also to abrupt changes in any higher derivative of the function that generates the data, which leads to an undesired loss of accuracy near critical points. A variety of solutions to handle this problem have been proposed; see for instance [1, 2, 10, 21]. However, none of them allows to unconditionally attain the optimal order of accuracy (that is, regardless of the order of the critical points) depending only on the local data without ending up with dimensional or scale-dependent weights. In other words, either some dimensional (namely, grid-size-dependent) or not properly scaled parameter is used, or data from

*Departament de Matemàtiques, Universitat de València, Av. Vicent Andrés Estellés, E-46100 Burjassot, Spain. E-Mail: antonio.baeza@uv.es

†CI²MA and Departamento de Ingeniería Matemática, Universidad de Concepción, Casilla 160-C, Concepción, Chile. E-mail: rburger@ing-mat.udec.cl

‡Departament de Matemàtiques, Universitat de València, Av. Vicent Andrés Estellés, E-46100 Burjassot, Spain. E-Mail: pep.mulet@uv.es

§CI²MA, Universidad de Concepción, Casilla 160-C, Concepción, Chile. E-Mail: dzorio@ci2ma.udec.cl

the global numerical solution are employed to define a non-dimensional and scale-independent parameter to prevent such loss of accuracy.

It is the purpose of this paper to design weights in such a way that the associated reconstruction algorithm does not lose accuracy in smooth zones, even in presence of critical points of any order. The decisive novelty of the new non-dimensional and scale-independent weights that only use information from the local data of the stencil. Since the order of accuracy of the resulting new WENO schemes is optimal, we refer to them as "optimal WENO" (OWENO) schemes. At the core of this paper is an analysis of the accuracy properties involving the asymptotics of the smoothness indicators as the grid size goes to zero. This issue has often been studied for reconstructions of specific orders along the literature, but no full proof for the general case has been advanced so far. We provide such a proof. The theoretical tools will be then available to fully and solidly analyze the accuracy of the reconstructions proposed, and are utilized to design OWENO reconstructions of unconditionally optimal order of accuracy regardless of the order of the critical points.

1.2. Related work. Overviews on WENO schemes include [16, 17, 22]. The particular problem of achieving optimal order of accuracy near critical points is tackled in many works. Henrick et al. [10] obtain optimal order convergence near critical points for the case of fifth order through a simple modification of the weights by Jiang and Shu [12], which involves mapping the weights to values that satisfy an optimality condition. The approach was further extended up to order 17 by Gerolymos et al. [8] and further enhanced by Feng et al. [7] by means of a different mapping. A different weight design was followed in the fifth-order WENO-Z method by Borges et al. [3], which attains fourth-order accuracy even at critical points. Castro et al. [4] extended the WENO-Z scheme to any odd order of accuracy, achieving optimal order at critical points by proper parameter tuning.

Following an idea similar to that of WENO-Z schemes, Yamaleev and Carpenter [21] introduced a new method, named ESWENO, based on the third-order case previously introduced in [20] that ensures energy stability in an L^2 norm. Even though it was not their primary goal to enhance order at critical points, it turns out that the resulting scheme achieves optimal order in the presence of critical points provided that the number of zero derivatives is at most the order of the scheme minus three. Another way to handle the problem of the order loss at critical points is the modification of the smoothness indicators. Ha et al. [9] proposed a new smoothness measurement that provides optimal order for functions with critical points, but in which the second derivative is not zero.

The design of weights in WENO schemes typically involves a quantity ε that avoids division by zero whenever an smoothness indicator becomes zero. This parameter was set to a fixed quantity $\varepsilon = 10^{-6}$ in [12], but Aràndiga et al. [1] noted that the choice of ε is crucial for the achievement of optimal order at critical points and that, for the case of the original weights of Jiang and Shu [12], the choice of ε proportional to the square of the mesh size provides the desired accuracy even at critical points. A similar analysis was later performed by Don and Borges [5], regarding WENO-Z schemes, and in [2] with respect to the ESWENO weights of Yamaleev and Carpenter (see also [13]), thus requiring a scale-dependent parameter.

1.3. Outline of this paper. The required theoretical background of this work is outlined in Section 2, where we derive bounds involving the asymptotical behaviour of the smoothness indicators as the grid size tends to zero. After collecting some preliminaries of notation in Subsection 2.1, we state in Subsection 2.2 some results that will be helpful for the analysis of the accuracy of WENO reconstructions for both cases of point value and cell average data. Such bounds are the key ingredients within Section 3, which is devoted to the definition of the new OWENO reconstructions that attain optimal order of accuracy regardless of the number of consecutive zero derivatives of the function to be reconstructed, and without using any scaling parameter. Inside this section, we first motivate the issues involving the accuracy loss of the existing schemes in the literature in Subsection 3.1. Then, we propose a novel smoothness indicator which overcomes these issues in Subsection 3.2, which is the main novelty of this paper, along with theoretical results that support the considerations on the optimal accuracy. Finally, Subsection 3.3 summarizes the algorithm of the proposed method with the novel smoothness indicators.

In summary, we prove that the new scheme has unconditionally optimal order of accuracy under those conditions, therefore overcoming the issue of the scheme proposed by Yamaleev and Carpenter [21] involving the accuracy loss near critical points in which the number of consecutive vanishing derivatives is the order of the scheme minus two. In Section 4 we present some numerical experiments, both for algebraic problems in Subsection 4.1 and problems involving hyperbolic conservation laws in Subsection 4.2. Finally, in Section 5 some conclusions are drawn. Some technical results related the accuracy of OWENO schemes are collected in Appendix A.

2. Regularity properties of functions and smoothness indicators. The analysis of WENO schemes will be carried out in one space dimension, where x denotes the spatial coordinate and $h>0$ is the uniform mesh width. This section is devoted to analyze the asymptotic accuracy properties of the smoothness indicators by Jiang and Shu [12], which on a stencil of $2r-1$ points $\{x_{-r+1},\dots,x_{r-1}\}$, with $x_{i+1}=x_i+h$, have the form

$$I=\sum_{l=1}^{r-1}\int_{x_0-h/2}^{x_0+h/2} h^{2l-1}\left(p^{(l)}(x)\right)^2\,\mathrm{d}x,$$

where p is a reconstruction polynomial, corresponding to a substencil of r points. The key result that lays the foundation for the ulterior accuracy analysis of the new OWENO reconstructions is Theorem 2.1, stated below, which provides the *exact* convergence rate of the Jiang-Shu smoothness indicators near critical points of any order. In order to prove this result, some technical definitions and results will be presented before. Theorem 2.1 is also crucial for the accuracy analysis near critical points of all the WENO reconstructions modalities presented in the literature that are based on the Jiang-Shu smoothness indicators.

2.1. Preliminaries. For a piecewise smooth function with jump discontinuities $f:\mathbb{R}\to\mathbb{R}$, we use the standard notation $f(h)=\mathcal{O}(h^\alpha)$ for $\alpha\in\mathbb{Z}$ to indicate the behaviour of a function f as $h\to 0$ in the standard sense, that is,

$$f(h)=\mathcal{O}(h^\alpha)\Leftrightarrow \limsup_{h\to 0}\left|f(h)h^{-\alpha}\right|<\infty.$$

Furthermore, we write $f(h)=\bar{\mathcal{O}}(h^\alpha)$ to express the more restrictive property

$$f(h)=\bar{\mathcal{O}}(h^\alpha)\Leftrightarrow \limsup_{h\to 0}\left|f(h)h^{-\alpha}\right|<\infty \quad\text{and}\quad \liminf_{h\to 0}\left|f(h)h^{-\alpha}\right|>0.$$

It follows for $\alpha,\beta\in\mathbb{Z}$ that $\bar{\mathcal{O}}(h^\alpha)^{-1}=\bar{\mathcal{O}}(h^{-\alpha})$, $\mathcal{O}(h^\alpha)\mathcal{O}(h^\beta)=\mathcal{O}(h^{\alpha+\beta})$ and $\bar{\mathcal{O}}(h^\alpha)\bar{\mathcal{O}}(h^\beta)=\bar{\mathcal{O}}(h^{\alpha+\beta})$. Moreover, we say that a function f has a critical point of order $k \geq 0$ at x if $f^{(l)}(x) = 0$ for $l = 1, \ldots, k$ and $f^{(k+1)}(x) \neq 0$. For $k = 0$ this includes the degenerate case of a point x at which $f'(x) \neq 0$.

We extend the classical notation for continuously higher differentiable function to denote by $f \in C^s(z)$ if there exists $\delta > 0$ such that $f \in C^s(z - \delta, z + \delta)$ and by $f \in C^s(z^{\pm})$ if there exists $\delta > 0$ such that f is s times continuously differentiable in $(z - \delta, z + \delta) \setminus \{z\}$ and $\lim_{x \to z^{\pm}} f^{(s)}(x) = f^{(s)}(z)$.

2.2. WENO reconstructions. For a stencil

$$S = \{x_{-r+1}, \ldots, x_{r-1}\} \tag{2.1}$$

of $2r - 1$ points $x_j = x_{j,h}$, where $x_{j+1} - x_j = h$ for $-r + 1 \leq j \leq r - 1$, and a scalar function f we assume that the data $\{f_{-r+1}, \ldots, f_{r-1}\}$ are either point values

$$f_j = f(x_j), \quad -r + 1 \leq j \leq r - 1, \tag{2.2}$$

or cell averages

$$f_j = \frac{1}{h} \int_{x_{j-1/2}}^{x_{j+1/2}} f(x)\, \mathrm{d}x, \quad -r + 1 \leq j \leq r - 1, \tag{2.3}$$

where in both cases we wish to approximate the point value $f(x_{1/2})$.

We denote by Π_k, $k \in \mathbb{N}_0$, the space of polynomials of *maximal* degree k, and by $\bar{\Pi}_k$ the space of polynomials of *exact* degree $k \in \mathbb{N}_0$. Let $p_{r,i} \in \Pi_{r-1}$ denote the reconstruction polynomial of the substencils

$$S_{r,i} = \{x_{-r+1+i}, \ldots, x_i\}, \quad 0 \leq i \leq r - 1, \tag{2.4}$$

with the interpolation property $p_{r,i}(x_j) = f_j$ for reconstructions from point values (2.2) or

$$\int_{x_{j-1/2}}^{x_{j+1/2}} p_{r,i}(x)\, \mathrm{d}x = f_j$$

for reconstructions from cell averages (2.3) for all $x_j \in S_{r,i}$. In what follows, we omit the subindex r when no confusion may arise.

The WENO strategy consists in defining a reconstruction q as a convex combination $q(x_{1/2}) = \omega_0 p_0(x_{1/2}) + \omega_1 p_1(x_{1/2}) + \cdots + \omega_{r-1} p_{r-1}(x_{1/2})$ of the individual reconstructions p_i with appropriately designed weights $\omega_0, \ldots, \omega_{r-1} \geq 0$, where $\omega_0 + \cdots + \omega_{r-1} = 1$, which satisfy $\omega_i \approx c_i$ on smooth zones, with c_i the linear ideal weights [1, Proposition 2], satisfying that $c_0 p_0(x_{1/2}) + c_1 p_1(x_{1/2}) + \cdots + c_{r-1} p_{r-1}(x_{1/2})$ coincides with the interpolatory polynomial of order $2r - 1$ at $x_{1/2}$. The weights ω_i are functions of some smoothness indicators, which we take according to Jiang and Shu [12]:

$$I_i = \sum_{l=1}^{r-1} \int_{x_{-1/2}}^{x_{1/2}} h^{2l-1} \big(p_i^{(l)}(x)\big)^2\, \mathrm{d}x. \tag{2.5}$$

Notice that $I_i = 0$ implies that $p_i' = 0$ on an interval of positive length, so that p_i' is zero everywhere, i.e., f is constant at the points of $S_{r,i}$.

THEOREM 2.1. *Let $z, \alpha \in \mathbb{R}$, $h > 0$ and $x_i = z + (\alpha + i)h$, $-r+1 \leq i \leq r-1$ define a stencil of equally-spaced nodes. If f has a critical point of order k at z, then the Jiang-Shu smoothness indicator (2.5) satisfies $I_i = \bar{\mathcal{O}}(h^{2\kappa})$, where*

$$\kappa = \begin{cases} \min\{l \in \mathbb{N} \colon 2|l, l \geq k, f^{(l+1)}(z) \neq 0\} & \text{for } r = 2 \text{ and } \alpha + i = 1/2, \\ k+1 & \text{otherwise.} \end{cases}$$

Proof. From Lemma A.2 applied to $n = r - 1$ and (A.7), we obtain

$$p_i^{(j)}(z + wh) = \sum_{s=j}^{m} b_{i,s,j}(w) h^{s-j} f^{(s)}(z) + \mathcal{O}(h^{m+1-j}), \tag{2.6}$$

where $b_{i,s,j}$ denotes the function $b_{s,j}$ given by Lemma A.2 corresponding to the stencil $S_{r,i}$. Notice that the condition $\alpha + i = 1/2$ is equivalent to $a_{0,i} = -a_{1,i}$. We apply (2.6) for $m = \kappa := \min\{\nu \in \mathbb{N} \colon b_{i,\nu,1}(w) f^{(\nu)}(z) \neq 0\}$. Then by the definition of k and Lemma A.2 we get for $j \leq \kappa_* := \min\{r-1, \kappa\}$:

$$p_{r,i}^{(j)}(z + wh) = b_{i,\kappa,j}(w) h^{\kappa-j} f^{(\kappa)}(z) + \mathcal{O}(h^{\kappa+1-j}). \tag{2.7}$$

We use the change of variables $x = z + wh$ to get from (2.7) for $j = 1$:

$$\int_{x_{-1/2}}^{x_{1/2}} \big(p_i^{(1)}(x)\big)^2 \mathrm{d}x = h^{2\kappa-1} \mu_{i,1} + \mathcal{O}(h^{2\kappa}),$$
$$\mu_{i,1} := \big(f^{(\kappa)}(z)^2\big) \int_{\alpha}^{\alpha+1} b_{i,\kappa,1}(w)^2 \mathrm{d}w > 0.$$

For $1 < j \leq \kappa$ (and, a fortiori, $r > 2$, therefore $\kappa = k+1$) we obtain

$$\int_{x_{-1/2}}^{x_{1/2}} \big(p_{r,i}^{(j)}(x)\big)^2 \mathrm{d}x = \mu_{i,j} h^{2(\kappa-j)+1} + \mathcal{O}(h^{2(\kappa-j)+2}),$$
$$\mu_{i,j} := \big(f^{(\kappa)}(z)\big)^2 \int_{\alpha}^{\alpha+1} \big(b_{i,\kappa,j}(w)\big)^2 \mathrm{d}w \geq 0.$$

For $j > \kappa$ we get

$$\int_{x_{-1/2}}^{x_{1/2}} \big(p_{r,i}^{(j)}(x)\big)^2 \mathrm{d}x = h \int_{x_{-1/2}}^{x_{1/2}} \big(b_{i,j,j}(w) f^{(j)}(z) + \mathcal{O}(h)\big)^2 \mathrm{d}w = \mathcal{O}(h).$$

The proof is complete after substituting these terms into (2.5):

$$\begin{aligned} I_i &= \sum_{j=1}^{\kappa_*} h^{2j-1} \big(\mu_{i,j} h^{2(\kappa-j)+1} + \mathcal{O}(h^{2(\kappa-j)+2})\big) + \sum_{j=\kappa_*+1}^{r-1} h^{2j-1} \mathcal{O}(h) \\ &= h^{2\kappa} \sum_{j=1}^{\kappa_*} \mu_{i,j} + \mathcal{O}(h^{2\kappa+1}), \end{aligned}$$

where we take into account that $\mu_{i,1} + \cdots + \mu_{i,\kappa_*} > 0$. ∎

3. Design of WENO weights. To define our modified scheme (the OWENO scheme), we design weights in such a way that the resulting scheme has the order of accuracy $2r-1$, for $r>2$, corresponding to WENO reconstructions of order at least 5. We do not consider the case $r=2$ since severe technical difficulties arise in the accuracy analysis, according to the results drawn in Theorem 2.1. This issue is very complex to address and will be tackled in full detail in a separate paper.

In WENO schemes, the weights ω_i are defined by a relation of the type

$$\omega_i = \alpha_i/(\alpha_0 + \cdots + \alpha_{r-1}), \quad 0 \le i \le r-1, \tag{3.1}$$

so that $\omega_0 + \cdots + \omega_{r-1} = 1$. In this section the quantities $\alpha_0, \ldots, \alpha_{r-1}$ are given by

$$\alpha_i = c_i \left(1 + \frac{d}{I_i^{s_1} + \varepsilon}\right)^{s_2}, \quad 0 \le i \le r-1, \tag{3.2}$$

for some $s_1, s_2 > 0$, $c_i > 0$ with $c_0 + \cdots + c_{r-1} = 1$ and where d is a function, to be defined below, that depends on $f_{-r+1}, \ldots, f_{r-1}$. This approach is related to Yamaleev and Carpenter [21]. The ultimate goal is to obtain the order of convergence $2r-1$, regardless of the presence of neighboring extrema [1, 2, 10, 21], and without assuming anything about the small number $\varepsilon > 0$ that ensures the strict positivity of the denominators. In contrast to other approaches [1, 2], our design does *not* rely on a functional relation between ε and h. Although $\varepsilon > 0$ is necessary if conditionals are to be avoided (which in turn may be necessary to avoid divisions by zero), our arguments will show that ε can be neglected in the asymptotical analysis of the order with respect to h.

3.1. Motivation. In the classical WENO order-enhancing argument in case of sufficient smoothness, for a function with an extremum of order k, the order of the reconstruction is

$$\mathrm{ord}_{\max} = \min\bigl\{\max\{2r-1, k+1\}, s + \max\{r, k+1\}\bigr\}, \tag{3.3}$$

where $\max\{2r-1, k+1\}$, resp. $\max\{r, k+1\}$, are the orders of the reconstructions with $p_{2r-1,r-1}$, resp. $p_{r,i}$ (see Lemma A.4) and $s \ge 0$ satisfies $\omega_i = c_i + \mathcal{O}(h^s)$. In what follows, we may assume $k \le 2r-3$, since otherwise (3.3) stipulates $\mathrm{ord}_{\max} = 2r-1$.

Yamaleev and Carpenter propose in [21] the following squared undivided difference of the $2r-1$ consecutive values $\{f_{-r+1}, \ldots, f_{r-1}\}$ to be used in (3.2) as term d:

$$d := d_1 := \Delta_{2r-2}(f_{-r+1}, \ldots, f_{r-1}) := \left(\sum_{j=-r+1}^{r-1} (-1)^{j+r-1} \binom{2r-2}{j+r-1} f_j\right)^2, \tag{3.4}$$

which has the following asymptotic accuracy properties:

$$\Delta_{2r-2}\bigl(f_{-r+1}, \ldots, f_{r-1}\bigr) = \begin{cases} \mathcal{O}(h^{4r-4}) & \text{if } f \in C^{2r-2}(z), \\ \bar{\mathcal{O}}(1) & \text{if } f \notin C^0(z). \end{cases} \tag{3.5}$$

Under the smoothness assumption, if we set $d = d_1^{s_1}$ in (3.2), then in view of $I_j = \bar{\mathcal{O}}(h^{2k+2})$ (cf. Theorem 2.1) we obtain $d_1^{s_1}/I_i^{s_1} = \mathcal{O}(h^{s_1(4r-2k-6)})$. The order-enhancing argument in this context requires that $d_1^{s_1}/I_i^{s_1} \to 0$ as $h \to 0$, which is not met if $k = 2r-3$. On the other hand, if $k \ge 2r-2$, then $\mathrm{ord}_{\max} \ge 2r-1$. So there remains an order loss gap at $k = 2r-3$. We herein close this gap by proposing an expression $d = D_r^{s_1}$, where the function $D_r = \Delta_{2r-2}(f_{-r+1},\dots,f_{r-1};\varepsilon)$ is designed such that the second-degree homogeneity property holds

$$\Delta_{2r-2}(\alpha f_{-r+1},\dots,\alpha f_{r-1};0) = \alpha^2 \Delta_{2r-2}(f_{-r+1},\dots,f_{r-1};0) \quad \text{for all } \alpha \in \mathbb{R}, \tag{3.6}$$

and that whenever $z_h = z + \mathcal{O}(h)$,

$$\Delta_{2r-2}\big(f_{-r+1},\dots,\alpha f_{r-1};0^+\big) = \begin{cases} \mathcal{O}(h^{4r-4}) & \text{if } f \in C^{2r-2}(z) \text{ and } k < 2r-3, \\ \mathcal{O}(h^{4r-3}) & \text{if } f \in C^{2r-2}(z) \text{ and } k = 2r-3, \\ \bar{\mathcal{O}}(1) & \text{if } f \notin C^0(z), \end{cases} \tag{3.7}$$

where $\Delta_{2r-2}(\cdot;0^+) := \lim_{\varepsilon\to 0^+} \Delta_{2r-2}(\cdot;\varepsilon)$.

Clearly, the previous analysis shows that the Yamaleev-Carpenter function d_1 in (3.4) satisfies (3.6), but fails to satisfy (3.7) by one order when $k = 2r-3$.

3.2. Novel smoothness indicator. The crucial contribution of this section, and the main novelty of this work, is the definition of a smoothness indicator that satisfies (3.6) and at the same time (3.7), namely, behaves like $\mathcal{O}(h^{4r-3})$, i.e., one order more than d_1, when $f \in C^{2r-2}(z)$ and $k = 2r-3$. This new smoothness indicator is defined by

$$d_2 := \Delta_{2r-2}(f_{-r+1,h},\dots,f_{r-1,h}) := B_h - 4A_hC_h, \tag{3.8}$$

where A_h, B_h and C_h are the coefficients of the parabola

$$P_h^{(2r-4)}(w) = A_h w^2 + B_h w + C_h,$$

which is the $(2r-4)$-th derivative of $P_h(w) = p_h(z+wh)$, where $p_h \in \Pi_{2r-2}$ is the reconstruction polynomial associated with the data $f_{-r+1,h},\dots,f_{r-1,h}$ and $f_{j,h} := z_h + jh$. Further details on the representation of the derivatives of P_h can be found in Lemma A.6. We state some properties of this new smoothness indicator prior to the definition of the parameter d in (3.2).

Proposition 3.1. *Let $n \geq 3$. With the same notation as in Lemma A.6, if $f \in C^0(z^\pm)$ is discontinuous at z, then $\Delta_n(f(x_{0,h}),\dots,f(x_{n,h})) = \bar{\mathcal{O}}(1)$.*

Proof. We let $f(z^-) =: f_{\mathrm{L}} \neq f_{\mathrm{R}} := f(z^+)$, where $f(z^\pm) := \lim_{y\to z^\pm} f(y)$, and define

$$i_0 := \begin{cases} \min\{0 \leq i \leq n \mid a_i \leq 0 \wedge a_{i+1} > 0\} & \text{if } f(z) = f_{\mathrm{L}}, \\ \min\{0 \leq i \leq n \mid a_i < 0 \wedge a_{i+1} \geq 0\} & \text{if } f(z) = f_{\mathrm{R}}, \end{cases} \qquad f_i := \begin{cases} f_{\mathrm{L}} & \text{if } i \leq i_0, \\ f_{\mathrm{R}} & \text{if } i > i_0. \end{cases}$$

If $p \in \bar{\Pi}_n$ is the interpolating polynomial with $p(z + a_ih) = f_i$, $0 \leq i \leq n$ and $P(w) := p(z+wh)$, then, by Lemma A.5, $P^{(n-2)}$ has two simple roots, and therefore $\Delta_n(f_0,\dots,f_n) > 0$. Since Δ_n is a continuous function (quadratic function with respect to their arguments) and $\lim_{h\to 0} f(x_{i,h}) = f_i$,

$$\lim_{h\to 0} \Delta_n\big(f(x_{0,h}),\dots,f(x_{n,h})\big) = \Delta_n(f_0,\dots,f_n) > 0,$$

hence $\Delta_n(f(x_{0,h}),\dots,f(x_{n,h})) = \bar{\mathcal{O}}(1)$. ∎

The following result is presented for a more general grid of the form $z_h + a_ih$, where z_h is assumed to satisfy $z_h = z + \mathcal{O}(h)$. This generalization implies that Δ_n

satisfies the desired bounds not only when the critical point is located in a relative position with respect to the stencil, but also when the stencil converges to the critical point (regardless of the relative position with respect to the critical point) as $h \to 0$. Namely, the following result stands for the behaviour of Δ_n *near* a critical point. This consideration is crucial in the context of partial differential equations (PDEs), in which the relative position of a critical point with respect to the stencils selected from the grid is arbitrary.

PROPOSITION 3.2. *Let $n \geq 3$ and assume that $f \in C^{n+1}(z)$ satisfies $f^{(n-1)}(z) = f^{(n-2)}(z) = 0$, $f^{(n)}(z) \neq 0$. Let $z_h \in \mathbb{R}$ such that $z_h - z = \mathcal{O}(h)$ and the stencil $x_{i,h} = z_h + a_i h$, $0 \leq i \leq n$, $a_0 < a_1 < \cdots < a_n$. Then there holds*

$$\Delta_n\big(f(x_{0,h}), \dots, f(x_{n,h})\big) = \mathcal{O}(h^{2n+1}).$$

Proof. By Lemma A.6, there holds

$$P_h^{(n-2)}(w) = \sum_{j=0}^{2} L_{\boldsymbol{a}}^{n-2,j}\big(f(x_{0,h}), \dots, f(x_{n,h})\big) w^j,$$

where $L_{\boldsymbol{a}}^{n-2,j} = L_{\boldsymbol{a}}^{n-2,j}(f(x_{0,h}), \dots, f(x_{n,h}))$, $j = 0, 1, 2$, satisfy

$$L_{\boldsymbol{a}}^{n-2,j}\big(f(x_{0,h}), \dots, f(x_{n,h})\big) = \frac{1}{j!} h^{n-2+j} f^{(n-2+j)}(z_h) + \mathcal{O}(h^{n+1}), \quad j = 0, 1, 2.$$

Denoting $\delta_h := z_h - z = \mathcal{O}(h)$, $A_h := L_{\boldsymbol{a}}^{n-2,2}$, $B_h := L_{\boldsymbol{a}}^{n-2,1}$, and $C_h := L_{\boldsymbol{a}}^{n-2,0}$, using Taylor expansion around z and considering that $f^{(n-2)}(z) = f^{(n-1)}(z) = 0$, we obtain

$$\begin{aligned}
A_h &= \frac{1}{2} h^n f^{(n)}(z_h) + \mathcal{O}(h^{n+1}) = \frac{1}{2} h^n f^{(n)}(z) + \mathcal{O}(h^{n+1}),\\
B_h &= h^{n-1} f^{(n-1)}(z_h) = \delta_h h^{n-1} f^{(n)}(z) + \mathcal{O}(h^{n+1}),\\
C_h &= h^{n-2} f^{(n-2)}(z_h) + \mathcal{O}(h^{n+1}) = \frac{1}{2} \delta_h^2 h^{n-2} f^{(n)}(z) + \mathcal{O}(h^{n+1}).
\end{aligned}$$

Therefore, the discriminant of the quadratic equation $P_h^{(n-2)}(w) = 0$ becomes

$$\begin{aligned}
B_h^2 - 4A_hC_h &= \delta_h^2 h^{2n-2} f^{(n)}(z)^2 \big((1 + \mathcal{O}(h^2))^2 - (1 + \mathcal{O}(h^3))(1 + \mathcal{O}(h))\big)\\
&= \mathcal{O}(h)^2 h^{2n-2} f^{(n)}(z)^2 \mathcal{O}(h) = \mathcal{O}(h^{2n+1}). \qquad \square
\end{aligned}$$

THEOREM 3.3. *Let $n \geq 3$, $z_h \in \mathbb{R}$ such that $z_h - z = \mathcal{O}(h)$, and consider the stencil $x_{i,h} = z_h + a_i h$, $0 \leq i \leq n$, $a_0 < a_1 < \cdots < a_n$. Then*

$$\Delta_n\big(f(x_{0,h}), \dots, f(x_{n,h})\big) =$$
$$= \begin{cases} \bar{\mathcal{O}}(1) & \text{if there exists } h_0 > 0 \text{ such that } x_{0,h} < z < x_{n,h} \\ & \text{for all } 0 < h < h_0 \text{, and } f \text{ has a discontinuity at } z, \\ \mathcal{O}(h^{2n+1}) & \text{if } f \in C^{n+1} \text{ with } f^{(l)}(z) = 0 \text{ for } 1 \leq l \leq n-1 \text{ and } f^{(n)}(z) \neq 0. \end{cases}$$

Proof. The result follows from Propositions 3.1 and 3.2, respectively. $\square$

We can now proceed to the definition of d appearing in (3.2), in a way such that the resulting reconstruction also attains optimal order near critical points of order $2r - 3$ (and thus of critical points of any order).

Let $p_h \in \Pi_n$, $n = 2r-2$, be the interpolating polynomial associated to the stencil S (see (2.1)). The $(n-2)$-th derivative of the polynomial $P_h(w) := p_h(z+wh)$ is a second-degree polynomial, which can be written as

$$P_h^{(n-2)}(w) = C_h + B_h w + A_h w^2,$$

where A_h, B_h, C_h are linear functions of $f_{-r+1}, \dots f_{r-1}$. Now, by Theorem 3.3 with $n = 2r-2$, the expression (3.8) satisfies

$$\Delta_{2r-2}\big(f_{-r+1}, \dots, f_{r-1}\big) = \begin{cases} \mathcal{O}(h^{4r-3}) & \text{if } f \in C^{2r-2}(z),\ k = 2r-3, \\ \bar{\mathcal{O}}(1) & \text{if } f \notin C^0(z). \end{cases} \tag{3.9}$$

For instance, for a WENO5 reconstruction ($r = 3$) from point values these terms can be written as

$$\begin{aligned} A_h &= \frac{1}{2}f_{-2} - 2f_{-1} + 3f_0 - 2f_1 + \frac{1}{2}f_2, \\ B_h &= -\frac{1}{2}f_{-2} + f_{-1} - f_1 + \frac{1}{2}f_2, \\ C_h &= -\frac{1}{12}f_{-2} + \frac{4}{3}f_{-1} - \frac{5}{2}f_0 + \frac{4}{3}f_1 - \frac{1}{12}f_2, \end{aligned}$$

while for reconstructions from cell averages the formula for C_h must be replaced by

$$C_h = -\frac{1}{8}f_{-2} + \frac{3}{2}f_{-1} - \frac{11}{4}f_0 + \frac{3}{2}f_1 - \frac{1}{8}f_2.$$

Based on (3.5) and (3.9), we define the function

$$D_r := d := \frac{d_1^{s_1}|d_2|^{s_1}}{d_1^{s_1} + |d_2|^{s_1} + \varepsilon} \tag{3.10}$$

related to the harmonic mean of $d_1^{s_1}$ and $d_2^{s_1}$. Its limit when $\varepsilon \to 0$, namely

$$\bar{d} = \begin{cases} \dfrac{d_1^{s_1}|d_2|^{s_1}}{d_1^{s_1} + |d_2|^{s_1}} & \text{if } d_1 d_2 \neq 0, \\ 0 & \text{otherwise,} \end{cases}$$

satisfies both desired properties, namely (3.6) and (3.7).

The asymptotics of the weights for $\varepsilon \to 0$ are analyzed in the Appendix and are used to obtain the following theorem.

Theorem 3.4. *If $f \in C^{2r-1}(z)$, $r \geq 3$, then*

$$f(x_{1/2}) - q(x_{1/2}) = \mathcal{O}(h^{2r-1}) + \mathcal{O}(\varepsilon^{s_2}).$$

Proof. We define $\bar{\omega}_i := \lim_{\varepsilon \to 0} \omega_i$ and $\bar{q}(x) := \bar{\omega}_0 p_0(x) + \cdots + \bar{\omega}_{r-1} p_{r-1}(x)$. The first step in the proof is to use Lemma A.3 to get for $e(h) = f(x_{1/2}) - \bar{q}(x_{1/2})$

$$\begin{aligned} f(x_{1/2}) - q(x_{1/2}) &= f(x_{1/2}) - \bar{q}(x_{1/2}) + \bar{q}(x_{1/2}) - q(x_{1/2}) \\ &= e(h) + \sum_{i=0}^{r-1}\big(\bar{\omega}_i - \omega_i\big)p_i(x_{1/2}) = e(h) + \sum_{i=0}^{r-1}\mathcal{O}(\varepsilon^{s_2})\mathcal{O}(1) = e(h) + \mathcal{O}(\varepsilon^{s_2}). \end{aligned}$$

It only remains to prove that

$$e(h)=\mathcal{O}(h^{2r-1}), \tag{3.11}$$

which will be achieved by analyzing the behavior of $\bar{\omega}_i$, for which we may assume that

$$\text{there exists } h_0>0 \text{ such that } I_j(h)\neq 0 \text{ for all } 0<h<h_0 \text{ and all } j, \tag{3.12}$$

since, otherwise, for each n there exist $h_n>0$ and $j_n\in\{0,\dots,r-1\}$ with

$$\lim_{n\to\infty} h_n=0,\quad I_{j_n}(h_n)=0.$$

It follows that f is constant on the points $\{x_{j,h_n}\}$, $j=-r+1+j_n,\dots,j_n$. Therefore there exists $\{z_n\}_{n\in\mathbb{N}}$ with $z_n\to z$ with $f'(z_n)=0$. A recursive use of Rolle's theorem and continuity yields that $f^{(k)}(z)=0$ for any $k=1,\dots,2r-1$, so Lemma A.4 yields $e(h)=\mathcal{O}(h^{2r-1})$.

We may assume that the order k of the critical point z, satisfies $k<2r-2$, since, otherwise, if $k\geq 2r-2$, then Lemma A.4 would yield that $e(h)=\mathcal{O}(h^{k+1})=\mathcal{O}(h^{2r-1})$ as in (3.11). Under this assumption and (3.12), from (A.4) we obtain

$$\bar{\omega}_i=c_i\left(\sum_{j=0}^{r-1}c_j\left(\frac{\beta_j}{\beta_i}\right)^{s_2}\right)^{-1},\quad \beta_i=1+\bar{d}/I_i^{s_1}. \tag{3.13}$$

Theorem 2.1 yields $I_j=\bar{\mathcal{O}}(h^{2(k+1)})$. By (3.10), (3.9) and (3.5) (in that order), we deduce that $d=\mathcal{O}(h^{s_1\nu})$, where $\nu=4r-4$ if $k<2r-3$ and $\nu=4r-3$ if $k=2r-3$. We analyze (3.13) with these estimates:

$$\left|\frac{\beta_j}{\beta_i}-1\right|=\frac{\bar{d}}{1+\bar{d}/I_i^{s_1}}\frac{|I_i^{s_1}-I_j^{s_1}|}{I_i^{s_1}I_j^{s_1}}\leq\frac{\bar{d}(I_i^{s_1}+I_j^{s_1})}{I_i^{s_1}I_j^{s_1}}=\frac{O(h^{\nu})\mathcal{O}(h^{(2(k+1))s_1})}{\bar{\mathcal{O}}(h^{4s_1(k+1)})},$$

which means that

$$\beta_j/\beta_i=1+\mathcal{O}(h^{\zeta}),\quad \zeta:=2s_1(\nu-k-1). \tag{3.14}$$

It follows from (3.13) that

$$\bar{\omega}_i=c_i\left(\sum_{j=0}^{r-1}c_j\left(1+\mathcal{O}(h^{\zeta})\right)^{s_2}\right)^{-1}=c_i\left(\sum_{j=0}^{r-1}c_j\left(1+\mathcal{O}(h^{\zeta})\right)\right)^{-1}=c_i+\mathcal{O}(h^{\zeta}). \tag{3.15}$$

Using that $\bar{\omega}_0+\cdots+\bar{\omega}_{r-1}=c_0+\cdots+c_{r-1}$, $f(z+h/2)-p_{2r-1,r-1}(z+h/2)=\mathcal{O}(h^{2r-1})$, and (A.5), we obtain from (3.15)

$$\begin{aligned}
e(h)=\sum_{i=0}^{r-1}\bar{\omega}_ie_i(h)&=\sum_{i=0}^{r-1}\big(c_i+\mathcal{O}(h^{\zeta})\big)\big(f(z+h/2)-p_i(z+h/2)\big)\\
&=\sum_{i=0}^{r-1}c_i\big(f(z+h/2)-p_i(z+h/2)\big)+\sum_{i=0}^{r-1}\mathcal{O}(h^{\zeta})\mathcal{O}\big(h^{\max\{r,k+1\}}\big)\\
&=f(z+h/2)-p(z+h/2)+\mathcal{O}\big(h^{\zeta+\max\{r,k+1\}}\big)\\
&=\mathcal{O}(h^{2r-1})+\mathcal{O}\big(h^{\zeta+\max\{r,k+1\}}\big)=\mathcal{O}\big(h^{\min\{2r-1,\zeta+\max\{r,k+1\}\}}\big).
\end{aligned}$$

Utilizing the definition of ζ in (3.14), one can easily verify that $\zeta+\max\{r,k+1\}\geq 2r-1$ for all $k\leq 2r-3$ and $s_1\geq 1$. ∎

REMARK 3.1. *All these precautions on the possibility of having smoothness indicators that vanish asymptotically are not void, since the function*

$$f(x) = \begin{cases} \mathrm{e}^{-1/x^2} & \text{for } x > 0, \\ 0 & \text{for } x \le 0 \end{cases}$$

satisfies $f \in C^\infty(\mathbb{R})$ *and* $f^{(n)}(0) = 0$ *for all* $n \in \mathbb{N}$*, therefore, for* $x = 0$*, it follows that* $I_0(h) = 0$ *for all* $h > 0$*.*

THEOREM 3.5. *If* f *has a discontinuity at* z *and is* r *times continuously differentiable in* $(z-\delta_0, z) \cup (z, z+\delta_0)$ *for some* $\delta_0 > 0$ *and is* r *times continuously differentiable either at* z^- *or at* z^+*, then*

$$f(x_{1/2}) - q(x_{1/2}) = \mathcal{O}\big(h^{\min\{r, 2s_1s_2\}}\big) + \mathcal{O}(\varepsilon^{s_2}).$$

Proof. We use the same notation and assume that $\varepsilon = 0$ as in the proof of Theorem 3.4 and aim to prove that $e(h) = \mathcal{O}(h^{\min\{r, 2s_1s_2\}})$. We define the index set

$$J_r := \big\{0 \le j \le r-1 : f|_{[x_{-r+1+j}, x_j]} \in C^r\big\}.$$

By the assumption on the lateral smoothness of f at z, since $z \in [x_{-r+1,j}, x_j]$ if and only if $-r+1+i \le (z-z_h)/h \le i$ and $(z-z_h)/h \in (-1,1)$, it follows that

$$\begin{cases} 0 \in J_r & \text{if } (z-z_h)/h \in (0,1) \text{ or } z = z_h = x_0 \text{ and } f \in C^r(z^-), \\ r-1 \in J_r & \text{if } (z-z_h)/h \in (-1,0) \text{ or } z = z_h = x_0 \text{ and } f \in C^r(z^+), \end{cases} \tag{3.16}$$

hence $J_r \neq \varnothing$.

The main difference with respect to Theorem 3.4 is that $I_j = \mathcal{O}(h^{m_j})$, where $m_j = 0$ if $j \notin J_r$ and $m_j = 2(k+1)$ if $j \in J_r$ and $d = \bar{\mathcal{O}}(1)$, which immediately yields

$$\frac{\beta_j}{\beta_i} = \frac{1 + d/I_j^{s_1}}{1 + d/I_i^{s_1}} = \bar{\mathcal{O}}\big(h^{(m_i - m_j)s_1}\big).$$

Therefore, for $i \notin J_r$, (3.13) reads

$$\begin{aligned} \bar{\omega}_i &= c_i \left(\sum_{j \in J_r} c_j \left(\frac{\beta_j}{\beta_i}\right)^{s_2} + \sum_{j \notin J_r} c_j \left(\frac{\beta_j}{\beta_i}\right)^{s_2} \right)^{-1} \\ &= c_i \left(\sum_{j \in J_r} c_j \big(\bar{\mathcal{O}}(h^{-2(k+1)s_1})\big)^{s_2} + \sum_{j \notin J_r} c_j \left(\bar{\mathcal{O}}(1)\right)^{s_2} \right)^{-1} \\ &= \frac{c_i}{\bar{\mathcal{O}}(h^{-2(k+1)s_1s_2}) + \bar{\mathcal{O}}(1)} = \frac{c_i}{\bar{\mathcal{O}}(h^{-2(k+1)s_1s_2})} = \mathcal{O}\big(h^{2(k+1)s_1s_2}\big) = \mathcal{O}\big(h^{2s_1s_2}\big) \end{aligned}$$

since $k \ge 0$. Since $\bar{\omega}_i \le 1$, $e_i(h) = \mathcal{O}(1)$ if $i \notin J_r$ and $e_i(h) = \mathcal{O}(h^r)$ if $i \in J_r$, we deduce

$$e(h) = \sum_{i=0}^{r-1} \bar{\omega}_i e_i(h) = \sum_{i \notin J_r} \mathcal{O}\big(h^{2s_1s_2}\big)\mathcal{O}(1) + \sum_{i \in J_r} \mathcal{O}(1)\mathcal{O}(h^r) = \mathcal{O}\big(h^{\min\{r, 2s_1s_2\}}\big). \quad \square$$

REMARK 3.2. *As a consequence of Theorem 3.5, we may take* $2s_1s_2 \ge r$ *to get the suboptimal* r*-th order at discontinuities.*

3.3. Summary of the algorithm. For the ease of reference we summarize here the new OWENO reconstruction for a local stencil.

Input: $\{f_{-r+1},\dots,f_{r-1}\}$ and $\varepsilon>0$.

1. Compute p_i, $0\le i\le r-1$, the corresponding reconstruction polynomials of degree $r-1$ at $x=x_{1/2}$. See [1, Proposition 1] for further details about their explicit expression.
2. Compute the Jiang-Shu smoothness indicators (2.5). See [1, Proposition 5] for further details about the explicit computation procedure to obtain their expression.
3. Compute d from (3.10) for $d_1:=\Delta_{2r-2}$ as given by (3.4), and $d_2:=\Delta_r$ as given in (3.8).
4. Compute the terms α_i from (3.2), where d is given by (3.10), with c_i the ideal linear weights, for some s_1,s_2 chosen by the user such that $s_1\ge 1$ and $s_2\ge r/(2s_1)$.
5. Generate the WENO weights $\omega_0,\dots,\omega_{r-1}$ from (3.1).
6. Obtain the OWENO reconstruction at $x_{1/2}$:

$$q_r(x_{1/2})=\omega_0p_0(x_{1/2})+\cdots+\omega_{r-1}p_{r-1}(x_{1/2}).$$

Output: $q_r(x_{1/2})$.

REMARK 3.3. *Since it is not guaranteed that $d_2\ge 0$, we included its absolute value $|d_2|$ in Equation (3.10). If one wants to avoid using an absolute value (and thus a Boolean condition in a WENO scheme), one has simply to chose an even s_1 satisfying the bounds in Remark 3.2.*

4. Numerical experiments. In this section, the chosen exponents are $s_1=2\lceil r/4\rceil$ (taking into account Remark 3.3), and $s_2=1$. The reason for this choice is that the choice of ε in (3.2) is related to the exponent s_2, since one should take $\varepsilon\gtrsim\varepsilon_0^{1/s_2}$, with ε_0 the lowest positive number of the working precision, in order to avoid arithmetic underflow/overflow. Moreover, although unnecessary according to the accuracy requirements in case of smoothness, the greater the parameter s_1 is, the closer are simultaneously the weights to the ideal weights in case of smoothness and to zero in case of discontinuity.

4.1. Algebraic test cases. We start our numerical tests with several numerical experiments devoted to emphasize the accuracy properties analyzed theoretically beforehand. We will perform tests involving JS-WENO (with the weight design by Jiang and Shu [12]), WENO-Z [4], YC-WENO [21] (with the improved version of the Yamaleev-Carpenter weight design [2]; and OWENO (with our design) reconstructions of order $2r-1$, with $2\le r\le 5$. All tests are performed with reconstructions both from cell average values to pointwise values and from pointwise values to pointwise values.

We perform these experiments by using the multiple-precision library MPFR [15] through its C++ wrapper [11], using a precision of 3322 bits ($\approx$ 1000 digits) and taking $\varepsilon=10^{-10^6}$ in all cases.

Example 1: Smooth problem. Let us consider the family of functions $f_k:\mathbb{R}\to\mathbb{R}$, $k\in\mathbb{N}$, given by $f_k(x)=x^{k+1}\mathrm{e}^x$. The function f_k has a critical point at $x=0$ of order k. Results involving the different values of r and k considered ($0\le k\le 2r-3$) are shown for $3\le r\le 5$ in Table 4.1 for the case of JS-WENO, YC-WENO and OWENO reconstructions. The error is given by $E_{k,n}=|P_N(0)-f_k(0)|$,

k	JS-WENO	WENO-Z	YC-WENO	OWENO	JS-WENO	WENO-Z	YC-WENO	OWENO
	Order 5 (from point values)				Order 5 (from cell averages)			
0	4.9915	5.0022	4.9983	4.9983	4.9909	5.0018	4.9983	4.9983
1	3.9742	5.0161	4.9980	4.9980	3.9802	5.0203	4.9981	4.9980
2	3.0198	2.9777	5.0331	5.0324	3.0348	2.9749	5.0324	5.0317
3	**3.9946**	**3.9945**	**3.9945**	**5.0056**	**3.9928**	**3.9927**	**3.9928**	**5.0035**
	Order 7 (from point values)				Order 7 (from cell averages)			
0	6.9902	6.9982	6.9984	6.9984	6.9899	6.9982	6.9984	6.9984
1	5.9743	7.0023	6.9981	6.9981	5.9699	7.0012	6.9981	6.9981
2	5.0494	7.0424	7.0002	7.0000	5.0432	7.0363	7.0001	6.9998
3	4.0005	4.0005	7.0627	7.0548	4.0001	4.0001	7.0600	7.0482
4	5.0747	5.0747	7.0040	7.0040	5.0655	5.0655	7.0108	7.0108
5	**6.0008**	**6.0008**	**6.0008**	**6.9907**	**6.0011**	**6.0011**	**6.0011**	**6.9980**
	Order 9 (from point values)				Order 9 (from cell averages)			
0	8.9831	8.9984	8.9984	8.9984	8.9829	8.9985	8.9985	8.9985
1	8.0225	8.9983	8.9983	8.9983	8.0226	8.9983	8.9983	8.9983
2	7.0368	9.0879	8.9981	8.9981	7.0229	9.0782	8.9981	8.9981
3	6.0712	9.0245	8.9978	8.9978	6.0625	9.0159	8.9978	8.9979
4	5.0133	5.0133	9.0628	8.9976	5.0072	5.0072	9.0625	8.9976
5	5.9855	5.9855	9.0325	9.0185	5.9815	5.9815	9.0283	9.0082
6	7.0409	7.0409	9.0121	9.0121	7.0746	7.0746	9.0143	9.0143
7	**7.9898**	**7.9898**	**7.9898**	**8.9541**	**7.9880**	**7.9880**	**7.9880**	**8.9872**

TABLE 4.1

Example 1 (smooth problem): Fifth-order, seventh-order, and ninth-order reconstructions. The cases in which both JS-WENO and YC-WENO methods lose accuracy (critical point of order $2r-3$) have been highlighted in bold text, in which it can be observed that the OWENO method keeps the optimal accuracy.

with P the corresponding reconstruction at $x_{1/2} = 0$, with the grid $x_i = (i - 1/2)h$, $-r+1 \leq i \leq r-1$, with $h = 1/N$ for $N \in \mathbb{N}$, when pointwise values (2.2) (with $f = f_k$) are taken, and pointwise values are reconstructed from pointwise values. Table 4.1 also presents the results for the same setup when cell average values (2.3) (with $f = f_k$) are taken instead and pointwise values are reconstructed from cell averages. In all cases Table 4.1 shows the corresponding average reconstruction orders

$$O_k = \frac{1}{80}\sum_{j=1}^{80} o_{k,j}, \quad \text{where} \quad o_{k,j} = \log_2\left(\frac{E_{k,N_{j-1}}}{E_{k,N_j}}\right), \quad N_j = 5 \cdot 2^j, \quad 0 \leq j \leq 80.$$

As we can see, the JS-WENO loses accuracy near critical points, presenting the order $r + |k - r + 1|$, with k the order of the critical point; also, WENO-Z presents the optimal $(2r-1)$-th order for $k < r-1$ and drops to order $k+1$ if $k \geq r-1$, whereas the YC-WENO reconstruction loses accuracy in the corner case $k = 2r-3$, as suggested in our theoretical considerations. In contrast, the OWENO reconstructions attain the optimal accuracy in all cases. This confirms that in practice the OWENO reconstruction is indeed able to overcome the loss of accuracy in all cases, including those in which YC-WENO-type reconstructions fail to attain the optimal accuracy.

Example 2: Discontinuous problem. We next test the accuracy of the methods with the same parameters as above for the function

$$f(x) = \begin{cases} \mathrm{e}^x & \text{if } x \leq 0, \\ \mathrm{e}^{x+1} & \text{if } x > 0, \end{cases}$$

where, in order to highlight the behaviour of the OWENO reconstructions at discontinuities, we change the location of the discontinuity by utilizing a grid of the form

θ	JS-WENO	WENO-Z	YC-WENO	OWENO	JS-WENO	WENO-Z	YC-WENO	OWENO
	Order 5 (from point values)				Order 5 (from cell averages)			
-2	2.9955	2.9952	2.9951	2.9917	2.9955	2.9952	2.9951	2.9929
-1	2.9927	2.9912	2.9925	2.9923	2.9935	2.9925	2.9934	2.9933
0	3.0029	3.0081	3.0045	3.0070	3.0033	3.0088	3.0050	3.0071
1	3.0271	3.0458	3.0390	3.0517	3.0294	3.0478	3.0411	3.0517
	Order 7 (from point values)				Order 7 (from cell averages)			
-3	3.9970	3.9980	4.0035	4.0140	3.9971	3.9982	4.0041	4.0297
-2	4.0088	4.0091	4.0089	4.0090	4.0071	4.0074	4.0072	4.0073
-1	3.9509	3.9487	3.9493	3.9473	4.0086	3.9479	4.0087	4.0088
0	4.0086	3.9412	4.0086	4.0086	4.0086	3.9407	4.0086	4.0086
1	4.0234	4.0234	4.0234	4.0234	4.0234	4.0235	4.0234	4.0235
2	4.0206	4.0257	4.0368	4.0344	4.0211	4.0261	4.0370	4.0353
	Order 9 (from point values)				Order 9 (from cell averages)			
-4	4.9937	4.9937	4.9937	4.9937	4.9938	4.9938	4.9938	4.9938
-3	4.9933	4.9933	4.9933	4.9933	4.9933	4.9933	4.9933	4.9933
-2	4.9928	4.9928	4.9928	4.9928	4.9927	4.9927	4.9927	4.9927
-1	4.9925	4.9924	4.9925	4.9825	4.9924	4.9923	4.9924	4.9924
0	4.9886	5.0631	4.9886	4.9886	4.9917	5.0634	4.9917	4.9917
1	5.0561	5.0561	5.0561	5.0561	5.0561	5.0561	5.0561	5.0561
2	5.0564	5.0564	5.0564	5.0564	5.0574	5.0574	5.0574	5.0574
3	5.0129	5.0356	5.0992	5.1073	5.0154	5.0373	5.1006	5.1042

Table 4.2

Example 2 (discontinuous problem): Fifth-order, seventh-order, and ninth-order reconstructions. The optimal accuracy is kept by all the reconstructions regardless of the location of the discontinuity.

$x_i = (i - 1/2 + \theta)h$, $-r + 1 \leq i \leq r - 1$, for $-r + 2 \leq \theta \leq r - 1$. Since $x_{1/2} = \theta h$, the error is now given by $|P(\theta h) - g(\theta h)|$. The results are shown in Table 4.2. Clearly, the suboptimal r-th order accuracy is also attained in all the cases when the data contain a discontinuity.

4.2. Experiments for conservation laws. In this section some numerical experiments involving hyperbolic conservation laws will be considered. For this purpose, we use a local Lax-Friedrichs (LLF) type flux splitting [18] for smooth problems, and Donat-Marquina's flux formula [6] for problems with weak solutions. On the other hand, for the time discretization, the approximate Lax-Wendroff schemes proposed by Zorío et al. [23] matching the spatial order will be considered. In this section we work in all experiments with double precision representation and set $\varepsilon = 10^{-100}$. For all schemes we consider fifth-order accuracy.

Example 3: Linear advection equation. We consider the linear advection equation with the following domain, boundary condition and initial condition:

$$\begin{aligned} &u_t + f(u)_x = 0, \quad \Omega = (-1, 1), \quad u(-1, t) = u(1, t), \\ &f(u) = u, \quad u_0(x) = 0.25 + 0.5 \sin(\pi x), \end{aligned}$$

whose exact solution is $u(x, t) = 0.25 + 0.5 \sin(\pi(x - t))$. We run several simulations with final time $T = 1$, for resolutions $h = 2/N$, $N \in \mathbb{N}$, using the classical JS-WENO, WENO-Z and YC-WENO schemes and the OWENO schemes, and compare them for the case of fifth-order accuracy, both with the L^1 and L^∞ errors. Since the characteristics point to the right, we use left-biased reconstructions. The results are shown in Table 4.3 for the fifth-order schemes. All schemes keep fifth-order accuracy. The results of the OWENO schemes are almost identical to those of the YC-WENO scheme.

	$\|\cdot\|_1$		$\|\cdot\|_\infty$		$\|\cdot\|_1$		$\|\cdot\|_\infty$	
N	Error	rate	Error	rate	Error	rate	Error	rate
	JS-WENO5				WENO-Z5			
10	8.44e-03	—	1.28e-02	—	1.22e-03	—	1.99e-03	—
20	3.59e-04	4.56	6.93e-04	4.20	3.27e-05	5.21	5.25e-05	5.24
40	1.09e-05	5.04	2.37e-05	4.87	1.01e-06	5.01	1.99e-03	5.04
80	3.29e-07	5.05	7.00e-07	5.08	3.15e-08	5.01	4.94e-08	5.01
160	1.02e-08	5.01	2.21e-08	4.98	9.79e-10	5.01	1.54e-09	5.01
320	3.19e-10	5.00	6.65e-10	5.06	3.05e-11	5.00	4.79e-11	5.00
640	9.96e-12	5.00	2.02e-11	5.04	9.52e-13	5.00	1.50e-12	5.00
	YC-WENO5				OWENO5			
10	1.02e-03	—	1.55e-03	—	9.52e-04	—	1.45e-03	—
20	3.27e-05	4.96	5.16e-05	4.91	2.95e-05	5.01	4.65e-05	4.96
40	1.01e-06	5.01	1.60e-06	5.01	9.03e-07	5.03	1.42e-06	5.03
80	3.15e-08	5.01	4.94e-08	5.01	2.78e-08	5.02	4.37e-08	5.02
160	9.79e-10	5.01	1.54e-09	5.01	8.63e-10	5.01	1.36e-09	5.01
320	3.05e-11	5.00	4.79e-11	5.00	2.68e-11	5.01	4.22e-11	5.01
640	9.52e-13	5.00	1.50e-12	5.00	8.37e-13	5.00	1.32e-12	5.00

TABLE 4.3

Example 3 (linear advection equation, solution at $T = 1$): fifth-order schemes.

	$\|\cdot\|_1$		$\|\cdot\|_\infty$		$\|\cdot\|_1$		$\|\cdot\|_\infty$	
N	Error	rate	Error	rate	Error	rate	Error	rate
	JS-WENO5				WENO-Z5			
40	6.28e-05	—	2.73e-04	—	7.99e-05	—	2.44e-04	—
80	3.14e-06	4.32	4.26e-05	2.68	6.08e-06	3.72	3.64e-05	2.75
160	1.55e-07	4.35	2.87e-06	3.89	4.05e-07	3.94	4.76e-06	2.94
320	9.44e-09	4.03	2.75e-07	3.38	2.63e-08	3.94	5.86e-07	3.02
640	5.38e-10	4.13	3.29e-08	3.06	1.66e-09	3.98	6.99e-08	3.07
1280	3.46e-11	3.96	3.58e-09	3.20	1.03e-10	4.01	8.22e-09	3.09
2560	2.10e-12	4.04	4.80e-10	2.90	6.37e-12	4.02	9.60e-10	3.10
	YC-WENO5				OWENO5			
40	2.55e-05	—	2.62e-04	—	2.49e-05	—	2.62e-04	—
80	8.46e-07	4.91	1.04e-05	4.65	8.46e-07	4.88	1.04e-05	4.65
160	2.62e-08	5.01	3.27e-07	4.99	2.62e-08	5.01	3.27e-07	4.99
320	7.97e-10	5.04	1.02e-08	5.00	7.97e-10	5.04	1.02e-08	5.00
640	2.45e-11	5.02	3.14e-10	5.02	2.45e-11	5.02	3.14e-10	5.02
1280	7.59e-13	5.01	9.71e-12	5.02	7.59e-13	5.01	9.71e-12	5.02
2560	2.34e-14	5.02	3.03e-13	5.00	2.34e-14	5.02	3.03e-13	5.00

TABLE 4.4

Example 4 (Burgers equation, smooth solution at $T = 0.3$): fifth-order schemes.

Examples 4 and 5: Burgers equation. We now consider the inviscid Burgers equation along with the following boundary and initial conditions:

$$\begin{aligned} &u_t + f(u)_x = 0, \quad \Omega = (-1,1), \quad u(-1,t) = u(1,t), \\ &f(u) = 0.5u^2, \quad u_0(x) = 0.25 + 0.5\sin(\pi x). \end{aligned} \tag{4.1}$$

In this case, $f(u_0(x))$ has a first-order critical point at $x = -1/2$ and $x = 1/2$. In Example 4, we consider the solution of (4.1) at $T = 0.3$, when it remains smooth, while in Example 5 we set $T = 12$, when the solution of (4.1) has become discontinuous. In Example 4 we run simulations for several resolutions, with an LLF flux splitting, and display the behaviour of the fifth-order schemes in Table 4.4. The exact solution is computed through a characteristic line method together with the Newton method, setting as tolerance double-precision machine accuracy. A loss of the order

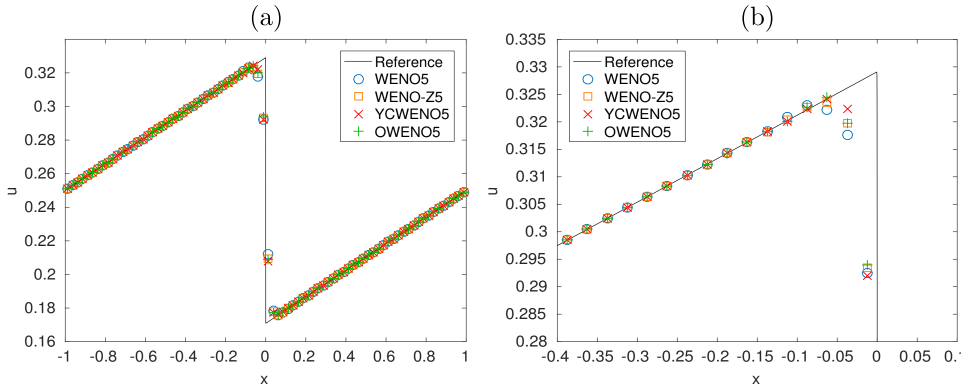

FIGURE 4.1. *Example 5 (Burgers equation, discontinuous solution at $T = 12$): fifth-order schemes.*

	$\|\cdot\|_1$		$\|\cdot\|_\infty$		$\|\cdot\|_1$		$\|\cdot\|_\infty$	
N	Error	rate	Error	rate	Error	rate	Error	rate
	JS-WENO5				WENO-Z5			
40	7.96e-05	—	5.17e-04	—	6.94e-05	—	5.14e-04	—
80	4.67e-06	4.09	7.31e-05	2.82	3.81e-06	4.19	7.29e-05	2.82
160	2.70e-07	4.11	9.73e-06	2.91	2.18e-07	4.13	9.70e-06	2.91
320	1.60e-08	4.08	1.25e-06	2.96	1.31e-08	4.05	1.25e-06	2.95
640	9.70e-10	4.04	1.59e-07	2.98	8.06e-10	4.03	1.59e-07	2.98
1280	5.95e-11	4.03	2.01e-08	2.99	4.99e-11	4.01	2.00e-08	2.99
2560	3.68e-12	4.02	2.52e-09	2.99	3.10e-12	4.01	2.51e-09	2.99
	YC-WENO5				OWENO5			
40	4.97e-05	—	3.15e-04	—	2.93e-05	—	2.01e-04	—
80	2.88e-06	4.11	5.58e-05	2.50	1.01e-06	4.86	9.83e-06	4.35
160	1.69e-07	4.09	7.98e-06	2.81	3.05e-08	5.05	3.42e-07	4.85
320	1.01e-08	4.06	1.06e-06	2.91	8.82e-10	5.11	1.22e-08	4.81
640	6.16e-10	4.03	1.36e-07	2.96	2.61e-11	5.08	3.95e-10	4.95
1280	3.81e-11	4.02	1.72e-08	2.98	7.91e-13	5.04	1.25e-11	4.99
2560	2.36e-12	4.01	2.17e-09	2.99	2.51e-14	4.98	3.90e-13	5.00

TABLE 4.5
Example 6 (customized equation, smooth solution at $T = 0.3$): fifth-order schemes.

of accuracy is observed for the JS-WENO and WENO-Z schemes. In contrast, the order of accuracy of the YC-WENO and all the OWENO schemes is optimal.

In Example 5 we run the simulation instead until $T = 12$. At $t = 1$, the wave breaks and a shock is generated. Therefore, in this case we use the Donat-Marquina flux-splitting algorithm [6]. The results are shown in Figure 4.1 with a resolution of $N = 80$ points, and are compared against a reference solution computed with $N = 16000$. This ranking of resolution is also consistent with the results for the smooth case.

Example 6: Customized equation with a third-order zero. We now consider the following initial-boundary value problem for a customized equation:

$$u_t + f(u)_x = 0, \quad \Omega = (-1, 1), \quad u(-1, t) = u(1, t),$$
$$f(u) = 0.5u^2 + 0.25u, \quad u_0(x) = 0.25 + 0.5\sin(\pi x).$$

In this case, $f(u_0(x))$ has a third-order critical point at $x = -1/2$ and a first-order critical point at $x = 1/2$. We now compare the behaviour of the three schemes with the same setup as in Example 4, by running a simulation until time $T = 0.3$, at which the solution is smooth. For the computation of the exact solution, we once again use the method of characteristic lines, with a Newton method matching the machine accuracy for the double precision. Since in this case the characteristics point always to the right, we use a left-biased upwind scheme. The results are shown in Table 4.5 for the fifth-order schemes. Clearly, the optimal order of accuracy is lost for both the JS-WENO, WENO-Z and YC-WENO schemes. In contrast, the fifth-order accuracy is solidly kept by the OWENO schemes. This is another confirmation, this time in the context of conservation laws, in which the OWENO are capable to handle the case $k = 2r - 3$, unlike the previously existing WENO schemes.

Example 7: Shu-Osher problem. The 1D Euler equations for gas dynamics are given by $\boldsymbol{u} = (\rho, \rho v, E)^{\mathrm{T}}$ and $\boldsymbol{f}(\boldsymbol{u}) = \boldsymbol{f}^1(\boldsymbol{u}) = (\rho v, p + \rho v^2, v(E + p))^{\mathrm{T}}$, where ρ is density, v is velocity, and E is the specific energy of the system. The pressure p is given by the equation of state $p = (\gamma - 1)(E - \rho v^2/2)$, where γ is the adiabatic constant that will be taken as $\gamma = 1.4$. We now consider the interaction with a Mach 3 shock and a sine wave. The spatial domain is now given by $\Omega := (-5, 5)$, with the initial condition

$$(\rho, v, p)(x, 0) = \begin{cases} (27/7, 4\sqrt{35}/9, 31/3) & \text{if } x \leq -4, \\ (1 + \sin(5x)/5, 0, 1) & \text{if } x > -4, \end{cases}$$

with left inflow and right outflow boundary conditions. This problem was first considered by Shu and Osher [19].

We run the simulation until $T = 1.8$ and compare the schemes against a reference solution computed with a resolution of $N = 16000$. Figures 4.2 (a) to (d) and (e) correspond to resolutions of $N = 200$ and $N = 400$ points, respectively. Both WENO-Z, YC-WENO and OWENO schemes produce similar resolutions, being the one presented by the OWENO scheme slightly higher. The lowest resolution clearly corresponds to the JS-WENO scheme, especially for the case $N = 200$. For $N = 400$ the OWENO5 scheme appears to capture the shock slightly better than the other schemes.

Finally, we show in Figure 4.2 (c) a comparison involving the error of each scheme with respect to the corresponding CPU time required to achieve it. We can see that the efficiency of all schemes is nearly the same in the case of fifth-order accuracy, although minor differences are found for lower resolution in benefit of both YC-WENO and OWENO schemes. Such asymptotic behaviour is probably due to the fact that there is no zero of order higher than one along the derivative of the composition of the flux with the solution. All the schemes considered can cope with the phenomena properly.

Example 8: Double Mach reflection problem. We consider a test problem for the 2D Euler equations:

$$\boldsymbol{u}_t + \boldsymbol{f}^1(\boldsymbol{u})_x + \boldsymbol{f}^2(\boldsymbol{u})_y = 0,$$

with

$$\boldsymbol{u} = \begin{pmatrix} \rho \\ \rho v^x \\ \rho v^y \\ E \end{pmatrix}, \quad \boldsymbol{f}^1(\boldsymbol{u}) = \begin{pmatrix} \rho v^x \\ p + \rho(v^x)^2 \\ \rho v^x v^y \\ v^x(E + p) \end{pmatrix}, \quad \boldsymbol{f}^2(\boldsymbol{u}) = \begin{pmatrix} \rho v^y \\ \rho v^x v^y \\ p + \rho(v^y)^2 \\ v^y(E + p) \end{pmatrix},$$

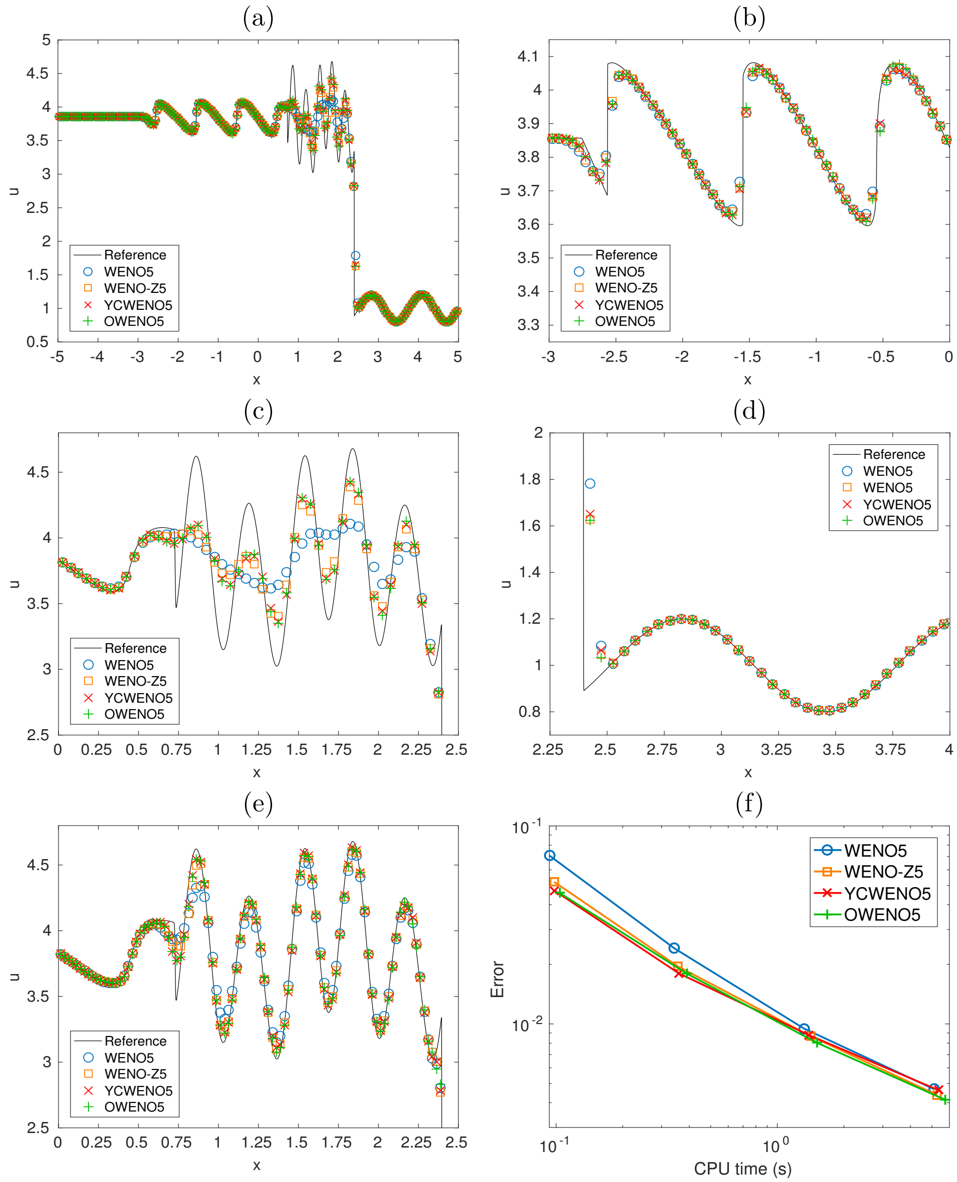

FIGURE 4.2. *Example 7 (Euler equations, Shu-Osher problem): numerical solutions at $T = 1.8$ by fifth-order schemes: (a) simulated density for spatial discretization $N = 200$, (b–d) enlarged views, (e) simulated density for $N = 400$, (f) efficiency plot.*

where ρ is density, (v^x, v^y) is velocity, E is the specific energy, and p is pressure. The equation of state is

$$p = (\gamma - 1)\left(E - \frac{1}{2}\rho((v^x)^2 + (v^y)^2)\right),$$

with $\gamma = 1.4$.

The Double Mach reflection test models a vertical right-going Mach 10 shock that

JS-WENO5	WENO-Z5	YC-WENO5	OWENO5
32.894029	34.199013	35.690326	36.847610

Table 4.6

Example 8 (Double Mach reflection problem, 128×32, 2D Euler equations of gas dynamics): CPU cost comparison (in seconds).

hits an equilateral triangle. By symmetry, we consider the problem defined only on the upper half part of the domain, which represents a collision of the shock with a ramp with a slope of 30° with respect to the horizontal line. Moreover, we consider the equivalent problem defined in a rectangle but with the shock rotated 30°. The domain is the rectangle $\Omega = [0,4] \times [0,1]$, and the initial conditions are given by

$$(\rho, v^x, v^y, E)(x,y,0) = \begin{cases} \boldsymbol{c}_1 = (\rho_1, v_1^x, v_1^y, E_1) & \text{if } y \leq 1/4 + \tan(\pi/6)x, \\ \boldsymbol{c}_2 = (\rho_2, v_2^x, v_2^y, E_2) & \text{if } y > 1/4 + \tan(\pi/6)x, \end{cases}$$

$$\boldsymbol{c}_1 = \big(8, 8.25\cos(\pi/6), -8.25\sin(\pi/6), 563.5\big), \quad \boldsymbol{c}_2 = (1.4, 0, 0, 2.5).$$

We impose inflow boundary conditions, with value $\boldsymbol{c}_1$, at the left side, $\{0\} \times [0,1]$, outflow boundary conditions both at $[0,1/4] \times \{0\}$ and $\{4\} \times [0,1]$, reflecting boundary conditions at $(1/4,4] \times \{0\}$ and inflow boundary conditions at the upper side, $[0,4] \times \{1\}$, which mimics the shock at its actual traveling speed:

$$(\rho, v^x, v^y, E)(x,1,t) = \begin{cases} \boldsymbol{c}_1 & \text{if } x \leq 1/4 + (1+20t)/\sqrt{3}, \\ \boldsymbol{c}_2 & \text{if } x > 1/4 + (1+20t)/\sqrt{3}. \end{cases}$$

We perform the simulations up to $T = 0.2$ for the fifth order versions of JS-WENO, WENO-Z, YC-WENO method and our OWENO scheme, at a resolution of 2560×640 points, with results shown in Figure 4.3. A value $CFL = 0.4$ has been used in all simulations. The results show that WENO-Z, YC-WENO and OWENO schemes produce sharper resolution than JS-WENO, with OWENO presenting a slightly higher resolution with respect to YC-WENO, and in turn YC-WENO presenting a slightly higher resolution than WENO-Z. Table 4.6 shows the CPU cost of the four schemes for the resolution of 128×32 points, in which it can be seen that the cost of all the involved schemes is similar.

5. Conclusions. We propose novel WENO reconstructions, called OWENO reconstructions, in which the accuracy is optimal regardless of the order of the critical point to which the stencil converges. The approach is related to the work by Yamaleev and Carpenter [21], We provide the necessary theoretical background to justify the properties of the scheme, which outperforms related existing methods under some circumstances, both for smooth and discontinuous solutions, and behave similarly under other situations. The fact that the new method does not always outperform existing ones is consistent with the conclusions drawn in [3], where it is claimed that improvements in the numerical solution mainly depend on how far from zero are the weights associated to stencils crossed by discontinuities, rather than to the detection of critical points (especially if they are high-order critical points). However, this work finally presents a WENO reconstruction procedure which never loses accuracy near critical points regardless of their order, relying only on the local data and without any influence of scaling parameters such as tuning the parameter ε. Therefore, it closes the question of the maximal order that can be attained near critical points by means

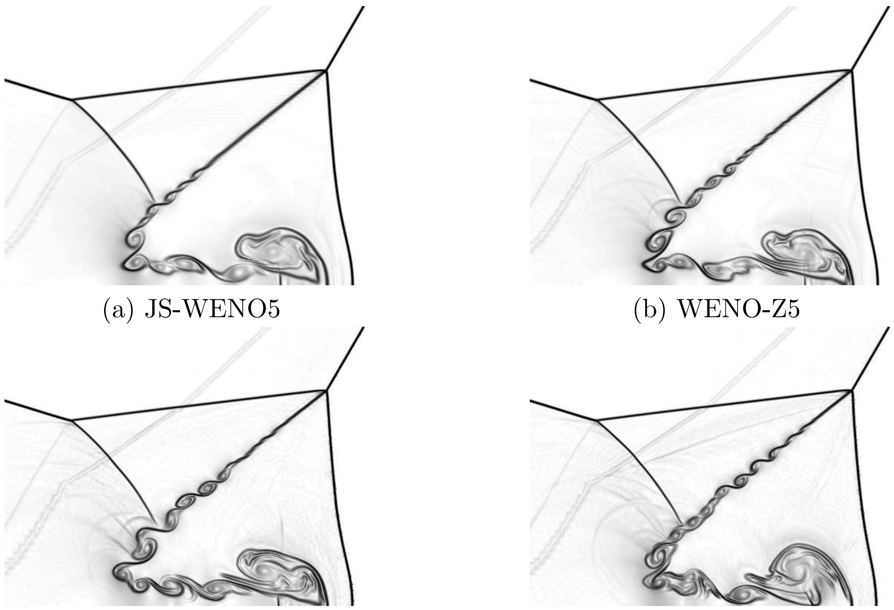

(a) JS-WENO5 (b) WENO-Z5

(c) YC-WENO5 (d) OWENO5

FIGURE 4.3. *Example 8 (Double Mach reflection problem,* 2560×640*, 2D Euler equations of gas dynamics): enlarged views of the turbulent zone of the numerical solutions at* $T = 0.2$ *(Schlieren plot).*

of WENO reconstructions. Some questions remain open, as for example the influence of the exponents s_1 and s_2 in the numerical dissipation and the determination their optimal values so as to reduce it as much as possible without generating artifacts or spurious oscillations.

Nevertheless, we expect a much more significant improvement for third-order schemes, whose original version proposed by Jiang and Shu [12] loses order near first-order critical points, which in this case, unlike higher-order critical points, is a very common phenomenon appearing in solutions of any type of ordinary differential equations (ODEs) or PDEs. Therefore, fixing this issue would entail a substantial improvement in the case of third-order WENO schemes. Since the procedure that we have described here is not valid for the case of third-order schemes, we are currently working on the development of a third order scheme with unconditionally optimal accuracy for smooth data.

Appendix A. Technical results. The following results are necessary for the development of the theoretical results presented in the main text, but their proofs being quite technical and involved, have been postponed to this appendix to enhance the readability of the main text.

The following result, whose proof follows by using Taylor expansion, is the key to proving Lemma A.2.

LEMMA A.1. *If* $\mathcal{L}\colon C^{m+1}[a,b] \to \Pi_n$ *is a linear and continuous operator with respect to* $\|\cdot\| = \|\cdot\|_\infty$*, then there exists* $K > 0$ *such that for any* $\zeta \in [a,b]$ *and*

$w \in [a, b]$,

$$\mathcal{L}[f](w) = \sum_{s=0}^{m} \frac{f^{(s)}(\zeta)}{s!}\mathcal{L}[(w-\zeta)^s] + \Delta_{m+1,\zeta}\mathcal{L}[f] \quad \text{with } \|\Delta_{m+1,\zeta}\mathcal{L}[f]\| \le K\,\|f^{(m+1)}\|.$$

LEMMA A.2. *Let $a_0 < a_1 < \cdots < a_n$ and z be fixed real numbers. Let $S = \{x_{0,h}, \ldots, x_{n,h}\}$ be an $(n+1)$-point stencil with $x_{i,h} = z + a_i h$ for $h > 0$. For any real function f, assume that the reconstruction polynomial $p_h = p_h[f] \in \Pi_n$ satisfies either $p_h(x_{i,h}) = f(x_{i,h})$ for $i = 0, \ldots, n$ or*

$$\int_{x_{i,h}-h/2}^{x_{i,h}+h/2} p_h(x)\,\mathrm{d}x = \int_{x_{i,h}-h/2}^{x_{i,h}+h/2} f(x)\,\mathrm{d}x \quad \text{for } i = 0, \ldots, n,$$

depending on whether the data are point values (2.2) or cell averages (2.3). Then, for $1 \le j \le n$ and $s \ge j$, there exist polynomials $b_{s,j} \in \Pi_{n-j}$, depending uniquely on the type of reconstruction and parameters $a_0, \ldots, a_n$, such that for any $f \in C^{m+1}$

$$p_h^{(j)}(z + wh) = \sum_{s=j}^{m} b_{s,j}(w) h^{s-j} f^{(s)}(z) + \mathcal{O}(h^{m+1-j}) \tag{A.1}$$

for sufficiently small wh. The functions $b_{s,j}$ have the following properties:

$$b_{s,j}(w) = s!\binom{s}{j} w^{s-j} \quad \text{for } j \le s \le n,$$

and $b_{s,1} \equiv 0$ if and only if $n = 1$, s is even and $a_0 = -a_1$, and $b_{s,1} \not\equiv 0$ otherwise.

Proof. We let $a = a_0 - 1/2$ and $b = a_n + 1/2$ and define the operators

$$\tilde{\mathcal{L}}_\nu, \mathcal{L}_{\nu,j} \colon C^{m+1}[a, b] \to \Pi_n, \quad \nu = 1, 2, \quad j \ge 1$$

through the following conditions, where $i = 0, \ldots, n$ and $j \le n$:

$$\tilde{\mathcal{L}}_1[f](a_i) = f(a_i), \qquad \mathcal{L}_{1,j}[f] = \big(\tilde{\mathcal{L}}_1[f]\big)^{(j)}, \tag{A.2}$$

$$\int_{a_i-1/2}^{a_i+1/2} \tilde{\mathcal{L}}_2[f](x)\,\mathrm{d}x = \int_{a_i-1/2}^{a_i+1/2} f(x)\,\mathrm{d}x, \qquad \mathcal{L}_{2,j}[f] = \big(\tilde{\mathcal{L}}_2[f]\big)^{(j)}. \tag{A.3}$$

The linearity of $\tilde{\mathcal{L}}_\nu$ and $\mathcal{L}_{\nu,j}$ is clear and the continuity can be proven by exploiting conditions (A.2) and (A.3), e.g., by using Lagrange basis polynomials φ_i (standard ones for point evaluation); i.e., if we define $\tilde{\mathcal{L}}_1[f] := f(a_0)\varphi_0 + \cdots + f(a_n)\varphi_n$, then

$$\mathcal{L}_{1,j}[f] = \sum_{i=0}^{n} f(a_i)\varphi_i^{(j)}, \quad \big\|\mathcal{L}_{1,j}[f]\big\| \le \max_{0 \le i \le n}(f(a_i)) \sum_{i=0}^{n}\big\|\varphi_i^{(j)}\big\| \le \|f\| \sum_{i=0}^{n}\big\|\varphi_i^{(j)}\big\|.$$

Similar arguments apply to the cell-average case ($\nu = 2$).

With the notation $S_{z,h}(w) := z + wh$, the polynomials (A.1) can be expressed as $p_h = \tilde{\mathcal{L}}[f \circ S_{z,h}] \circ S_{z,h}^{-1}$, which means that $p_h(x) = \tilde{\mathcal{L}}[f \circ S_{z,h}]((x-z)/h)$, where either $\tilde{\mathcal{L}} = \tilde{\mathcal{L}}_1$ or $\tilde{\mathcal{L}} = \tilde{\mathcal{L}}_2$, and correspondingly, either $\mathcal{L}_j = \mathcal{L}_{1,j}$ or $\mathcal{L}_j = \mathcal{L}_{2,j}$. Since $(f \circ S_{z,h})^{(s)}(w) = h^s f^{(s)}(z + wh)$, Lemma A.1 for $\zeta = 0$ yields

$$p_h^{(j)}(x) = h^{-j}\tilde{\mathcal{L}}[f \circ S_{z,h}]^{(j)}\big((x-z)/h\big) = h^{-j}\mathcal{L}_j[f \circ S_{z,h}]\big((x-z)/h\big),$$

$$
\begin{aligned}
p_h^{(j)}(z+wh) &= h^{-j}\mathcal{L}_j[f\circ S_{z,h}](w)\\
&= h^{-j}\sum_{s=0}^{m}\frac{(f\circ S_{z,h})^{(s)}(0)}{s!}\mathcal{L}_j[w^s] + h^{-j}\Delta_{m+1,0}\mathcal{L}_j[f\circ S_{z,h}]\\
&= \sum_{s=j}^{m} h^{s-j}\frac{f^{(s)}(z)}{s!}\mathcal{L}_j[w^s] + \mathcal{O}(h^{m+1-j}),
\end{aligned}
$$

since $\tilde{\mathcal{L}}[w^s]=w^s$ for $s\leq n$, therefore $\mathcal{L}_j[w^s]=(\tilde{\mathcal{L}}[w^s])^{(j)}=0$ for $s<j$, and

$$
\Delta_{m+1,0}\mathcal{L}_j[f\circ S_{z,h}] \leq K\big\|(f\circ S_{z,h})^{(m+1)}\big\|_{[a,b]} = Kh^{m+1}\big\|f^{(m+1)}\big\|_{S_{z,h}([a,b])}.
$$

Therefore, the result follows with $b_{s,j}(w)=\mathcal{L}_j[w^s]/s!$.

Finally, if $n\geq 1$ and $b_{s,1}(w)=0$, then for the first operator we have

$$
\tilde{\mathcal{L}}_1[w^s]=\alpha \Leftrightarrow a_i^s=\alpha,\ i=0,\dots,n \Leftrightarrow n=1,\ s \text{ is even and } a_0=-\alpha^{1/s},\ a_1=\alpha^{1/s}.
$$

For the second operator, we have $b_{s,1}(w)=0\Leftrightarrow$

$$
\tilde{\mathcal{L}}_2[w^s]=\alpha \Leftrightarrow q_s(a_i)=(a_i+1/2)^{s+1}-(a_i-1/2)^{s+1}=(s+1)\alpha, \quad i=0,\dots,n,
$$

where we define

$$
q_s(x) := (x+1/2)^{s+1}-(x-1/2)^{s+1} = \sum_{l=0}^{\lfloor s/2\rfloor}\binom{s+1}{2l+1}\frac{1}{2^{2l}}x^{s-2l}.
$$

Thus, by Rolle's theorem, there exist numbers $\tilde{a}_i\in(a_{i-1},a_i)$, $i=1,\dots,n$ such that $q_s'(\tilde{a}_i)=0$. But

$$
q_s'(x) = \sum_{l=0}^{\lfloor s/2\rfloor}\binom{s+1}{2l+1}\frac{1}{2^{2l}}(s-2l)x^{s-2l-1}
$$

has only even-degree terms, with strictly positive coefficients, when s is odd (and therefore no roots) and only odd-degree terms, with strictly positive coefficients, when s is even (and therefore 0 as only root). This implies that s is even, $n=1$ and $\tilde{a}_1=0$, which yields $a_0<\tilde{a}_1=0<a_1$. Since q_s is an even function and strictly increasing in $(0,\infty)$, for even s, $q_s(a_0)=q_s(-a_0)=q_s(a_1)$ implies $a_1=-a_0$. The converse is clear, since $n=1$, $a_1=-a_0$ and even s implies that $q_s(a_1)=q_s(a_0)=\alpha$ and therefore $\tilde{\mathcal{L}}_2[w^s]=\alpha$ and $b_{s,1}(w)=(1/s!)\tilde{\mathcal{L}}_2[w^s]'=0$. ∎

After some straightforward algebra, we prove in the next result that $\bar{\omega}_i=\lim_{\varepsilon\to 0}\omega_i$ exists and we obtain its rate of convergence.

Lemma A.3. *For fixed data $f_{-r+1},\dots,f_{r-1}$, we have $\omega_i=\bar{\omega}_i+\mathcal{O}(\varepsilon^{s_2})$ and*

$$
\bar{\omega}_i = \begin{cases}
c_i & \text{if } d_1d_2=0,\\
\dfrac{c_i}{\sum_{j=0,I_j\neq 0}^{r-1} c_j} & \text{if } d_1d_2\neq 0,\ \exists k \text{ with } I_k=0, \text{ and } I_i=0,\\
0 & \text{if } d_1d_2\neq 0,\ \exists k \text{ with } I_k=0, \text{ and } I_i\neq 0,\\
\dfrac{c_i\big(1+\bar{d}/I_i^{s_1}\big)^{s_2}}{\sum_{j=0}^{r-1} c_j\big(1+\bar{d}/I_j^{s_1}\big)^{s_2}} & \text{if } d_1d_2\neq 0 \text{ and } I_k\neq 0 \text{ for } k=0,\dots,r-1.
\end{cases} \tag{A.4}
$$

LEMMA A.4. *If $f \in C^s(z)$ and $f^{(s')}(z) = 0$ for all $s' < s$, then*

$$e_i(h) := f(z + h/2) - p_i(z + h/2) = \mathcal{O}(h^{\max\{r,s\}}), \tag{A.5}$$

$$e(h) := f(z + h/2) - q(z + h/2) = \mathcal{O}(h^{\max\{r,s\}}). \tag{A.6}$$

Proof. We prove the result for the interpolatory case, the cell-average case is similar. Without loss of generality assume $z = 0$. Using the Newton representation of the interpolation error, we get

$$e_i(h) = f(x_{1/2}) - p_i(x_{1/2}) = \frac{f^{(r)}(\xi)}{r!} h^r \prod_{l=0}^{r-1} \left(\frac{1}{2} - i + l\right),$$

where $|\xi - z| < \max\{r - 1 - i, i\}h < rh$. The result follows for $s \le r$. For $s > r$, due to the assumption and using Taylor's remainder theorem, we get

$$f^{(r)}(\xi) = \frac{f^{(s)}(\xi_{s,r})}{(s-r)!}(\xi - z)^{s-r} |\xi_{s,r} - z| < |\xi - z|.$$

It follows that for sufficiently small h_0,

$$\left|e_i(h)\right| \le \max_{|\xi - z| < rh_0} \left|f^{(s)}(\xi)\right| \frac{r^s}{r!(s-r)!} h^s \quad \text{for } 0 < h < h_0.$$

This concludes the proof of (A.5), and (A.6) follows from $\bar{\omega}_0 + \cdots + \bar{\omega}_{r-1} = 1$. ◻

In order to use the previous results, we consider $x_{i,h} = z + (\alpha + i)h$, with $\alpha \in \mathbb{R}$ fixed and $i \in \mathbb{Q}$, so that, for instance $x_{1/2,h} = z + (\alpha + 1/2)h$. The reconstruction polynomial $p_{r,i}$ associated to the substencil $S_{r,i}$ (see (2.4)) corresponds to p_h in Lemma A.2 for $n = r - 1$ and

$$a_j = a_{j,i} := \alpha - r + i + 1 + j, \quad j = 0, \ldots, r-1. \tag{A.7}$$

LEMMA A.5. *Let $x_0 < x_1 < \cdots < x_n$ be a stencil. Let $0 \le i_0 \le n-1$ and $p \in \Pi_n$ be an interpolating polynomial such that $p(x_i) = f_{\mathrm{L}}$ if $i \le i_0$ and $p(x_i) = f_{\mathrm{R}}$ if $i > i_0$, with $f_{\mathrm{L}} \ne f_{\mathrm{R}}$. Then, $p^{(s)}$ has exactly $n - s$ roots, for $1 \le s \le n$, and $p^{(s)} \in \bar{\Pi}_{n-s}$ for $0 \le s \le n$. In particular, the parabola $p^{(n-2)}$ has two simple roots.*

Proof. Let $0 \le i \le n-1$ such that $i \ne i_0$. Then, by construction, we have $p(x_i) = p(x_{i+1})$, and therefore by Rolle's theorem exists $\xi_i \in (x_i, x_{i+1})$ such that $p'(\xi_i) = 0$, $0 \le i \le n-1$. Therefore, $p' \in \Pi_{n-1}$ has at least $n-1$ roots. However, since p takes different values it is not a constant polynomial, and thus $p' \not\equiv 0$. Hence, $p' \in \bar{\Pi}_{n-1}$, p' must have exactly $n-1$ roots and, a fortiori, $p \in \bar{\Pi}_n$. A recursive application of Rolle's theorem yields that $(p')^{(s-1)} = p^{(s)} \in \bar{\Pi}_{n-1-(s-1)} = \bar{\Pi}_{n-s}$ has exactly $(n-1) - (s-1) = n - s$ roots for $1 \le s \le n$. ◻

LEMMA A.6. *Let $x_{i,h} = z + a_i h$, $0 \le i \le n$, be a grid with $a_0 < a_1 < \cdots < a_n$ and $p_h \in \Pi_n$ the interpolating polynomial such that $p_h(x_{i,h}) = f_i$, for $f_i \in \mathbb{R}$, $0 \le i \le n$. Then, given $0 \le s \le n$, the s-th derivative of $P_h(w) := p_h(z + wh)$ can be written as*

$$P_h^{(s)}(w) = \sum_{j=0}^{n-s} L_{\boldsymbol{a}}^{s,j}(f_{0,h}, \ldots, f_{n,h}) w^j, \quad \boldsymbol{a} := (a_0, \ldots, a_n),$$

with $L_{\boldsymbol{a}}^{s,j} : \mathbb{R}^{n+1} \to \mathbb{R}$ a linear function, which does not depend on h. Furthermore,

$$L_{\boldsymbol{a}}^{s,j}(f_{0,h}, \ldots, f_{n,h}) = \frac{(s+j)!}{j!} L_{\boldsymbol{a}}^{0,s+j}(f_{0,h}, \ldots, f_{n,h}). \tag{A.8}$$

Moreover, if $f_i = f(x_{i,h})$, for some $f \in C^{n+1}$, then

$$L_{\boldsymbol{a}}^{s,j}(f_{0,h}, \dots, f_{n,h}) = \frac{h^{s+j}}{j!} f^{(s+j)}(z) + \mathcal{O}(h^{n+1}).$$

Proof. Let $\mathcal{F}$ be the vector space of real functions and $\Phi_{\boldsymbol{a}} \colon \mathcal{F} \to \mathbb{R}^{n+1}$ be the linear function given by $\Phi_{\boldsymbol{a}}(f) = (f(a_0), \dots, f(a_n))$. Since $\ker \Phi_{\boldsymbol{a}} \cap \Pi_n = 0$, and $\dim \Pi_n = n+1$, $\Phi_{\boldsymbol{a}}|_{\Pi_n}$ is a bijection and $P_h = (\Phi_{\boldsymbol{a}}|_{\Pi_n})^{-1}(f_{0,h}, \dots, f_{n,h})$. Since $\pi_i \colon \Pi_n \to \mathbb{R}$, $\pi_i(\sum_{j=0}^n \alpha_j w^j) = \alpha_i$ is a linear function, $\pi_i \circ (\Phi_{\boldsymbol{a}}|_{\Pi_n})^{-1}$ is also a linear function, therefore

$$P_h(w) = \sum_{j=0}^n L_{\boldsymbol{a}}^{0,j}(f_{0,h}, \dots, f_{n,h}) w^j, \quad L_{\boldsymbol{a}}^{0,j} = \pi_i \circ (\Phi_{\boldsymbol{a}}|_{\Pi_n})^{-1},$$

from where equation (A.8) follows immediately.

Assume $f_i = f(x_{i,h})$, $f \in C^{n+1}(z)$. Since $p_h(x) = P_h((x-z)/h)$,

$$p_h(x) = \sum_{j=0}^n L_{\boldsymbol{a}}^{0,j}(f_{0,h}, \dots, f_{n,h}) h^{-j} (x-z)^j.$$

This yields $L_{\boldsymbol{a}}^{0,j}(f_{0,h}, \dots, f_{n,h}) h^{-j} j! = p_h^{(j)}(z)$, for $j = 0, \dots, n$. On the other hand the interpolation property yields $p_h^{(j)}(z) = f^{(j)}(z) + \mathcal{O}(h^{n+1-j})$, for $j = 0, \dots, n$, thus implying

$$L_{\boldsymbol{a}}^{0,j}(f_{0,h}, \dots, f_{n,h}) = \frac{f^{(j)}(z)}{j!} h^j + \mathcal{O}(h^{n+1}),$$

which, together with (A.8), concludes the proof. ∎

Acknowledgements. AB, PM and DZ are supported by Spanish MINECO project MTM2017-83942-P. RB is supported by CRHIAM, project CONICYT/FONDAP/15130015; CONICYT/PIA/AFB170001; and Fondecyt project 1170473. PM is also supported by Conicyt (Chile), project PAI-MEC, folio 80150006. DZ is also supported by Conicyt (Chile) through Fondecyt project 3170077.

REFERENCES

[1] F. Aràndiga, A. Baeza, A.M. Belda, and P. Mulet, *Analysis of WENO schemes for full and global accuracy*, SIAM J. Numer. Anal., 49 (2011), pp. 893–915.

[2] F. Aràndiga, M.C. Martí, and P. Mulet, *Weights design for maximal order WENO schemes*, J. Sci. Comput., 60 (2014), pp. 641–659.

[3] R. Borges, M. Carmona, B. Costa, and W.S. Don, *An improved weighted essentially non-oscillatory scheme for hyperbolic conservation laws*, J. Comput. Phys., 227 (2008), pp. 3191–3211.

[4] M. Castro, B. Costa, and W.S. Don, *High order weighted essentially non-oscillatory WENO-Z schemes for hyperbolic conservation laws*, J. Comput. Phys., 230 (2011), pp. 1766–1792.

[5] W.-S. Don and R. Borges, *Accuracy of the weighted essentially non-oscillatory conservative finite difference schemes*, J. Comput. Phys., 250 (2013), pp. 347–372.

[6] R. Donat and A. Marquina, *Capturing shock reflections: An improved flux formula*, J. Comput. Phys., 125 (1996), pp. 42–58.

[7] H. Feng, F. Hu, and R. Wang, *A new mapped weighted essentially non-oscillatory scheme*, J. Sci. Comput., 51 (2012), pp. 449–473.

[8] G.A. Gerolymos, D. Sénéchal, and I. Vallet, *Very-high-order WENO schemes*, J. Comput. Phys., 228 (2009), pp. 8481–8524.

[9] Y. Ha, C.H. Kim, Y.J. Lee, and J. Yoon, *An improved weighted essentially non-oscillatory scheme with a new smoothness indicator*, J. Comput. Phys., 232 (2013), pp. 68–86.
[10] A.K. Henrick, T.D. Aslam, and J.M. Powers, *Mapped weighted essentially non-oscillatory schemes: Achieving optimal order near critical points*, J. Comput. Phys., 207 (2005), pp. 542–567.
[11] P. Holoborodko, *MPFR C++*, http://www.holoborodko.com/pavel/mpfr/
[12] G.S. Jiang and C.-W. Shu, *Efficient implementation of Weighted ENO schemes*, J. Comput. Phys., 126 (1996), pp. 202–228.
[13] O. Kolb, *On the full and global accuracy of a compact third order WENO scheme*, SIAM J. Numer. Anal., 52 (2014), pp. 2335–2355.
[14] X.-D. Liu, S. Osher, and T. Chan, *Weighted essentially non-oscillatory schemes*, J. Comput. Phys., 115 (1994), pp. 200–212.
[15] *The GNU MPFR library*, http://www.mpfr.org/
[16] C.-W. Shu, *Essentially non-oscillatory and weighted essentially non-oscillatory schemes for hyperbolic conservation laws.* In B. Cockburn, C. Johnson, C.-W. Shu, and E. Tadmor (A. Quarteroni, ed.), *Advanced Numerical Approximation of Nonlinear Hyperbolic Equations*, Lecture Notes in Mathematics vol. 1697, Springer-Verlag, Berlin (1998), pp. 325–432.
[17] C.-W. Shu, *High order weighted essentially nonoscillatory schemes for convection dominated problems*, SIAM Rev., 51 (2009), pp. 82–126.
[18] C.-W. Shu and S. Osher, *Efficient implementation of essentially non-oscillatory shock-capturing schemes*, J. Comput. Phys., 77 (1988), pp. 439–471.
[19] C.-W. Shu and S. Osher, *Efficient implementation of essentially non-oscillatory shock-capturing schemes, II*, J. Comput. Phys., 83 (1989), pp. 32–78.
[20] N.K. Yamaleev and M.H. Carpenter, *Third-order Energy Stable WENO scheme*, J. Comput. Phys. 228 (2009), pp. 3025–3047.
[21] N.K. Yamaleev and M.H. Carpenter, *A systematic methodology to for constructing high-order energy stable WENO schemes*, J. Comput. Phys., 228 (2009), pp. 4248–4272.
[22] Y.-T. Zhang and C.-W. Shu, *ENO and WENO schemes*, Chapter 5 in R. Abgrall and C.-W. Shu, C.-W. (eds.), *Handbook of Numerical Methods for Hyperbolic Problems: Basic and Fundamental Issues*. Handbook of Numerical Analysis vol. 17, North Holland, (2016), pp. 103–122.
[23] D. Zorío, A. Baeza, and P. Mulet, *An approximate Lax-Wendroff-type procedure for high-order accurate schemes for hyperbolic conservation laws*, J. Sci. Comput., 71 (2017), pp. 246–273.